INTELLIGENT TOWERS FOR ELECTROMAGNETIC SHOWERS*

C. Blocker, G. W. Brandenburg, R. Carey, T. Edberg,
M. Levi, J. Oliver, N. Patz, E. Sadowski, T. Schaad, R. Schwitters
Harvard University
High Energy Physics Laboratory
Cambridge, MA 02138

Gas tube calorimetry is an attractive alternative to the methods entailing light collection. It is possible to design calorimeters with a flexible geometry and fine granularity for a lower cost than those having complicated light guides and many phototubes. Although the energy resolution is not as good for the gas tube counters, it is perfectly adequate for applications in the multi-GeV range.

We have designed and tested a gas-tube calorimeter that incorporates the modularity and tower structure of a lead glass block array. We combine the signals from the individual tubes using a resistive weighting technique to obtain the transverse moments of the energy distribution within a tower or block. These moments provide excellent position and angle information about the shower as well as π^o/γ separation. This design could prove valuable in applications where a large area electromagnetic calorimeter is needed downstream of a high energy interaction point. One application we have considered is to cover the small angle region in a high energy colliding beam experiment.

The basic element in our detector is a 5½" x 5½" x 12" (16 r.l.) shower tower containing twenty alternating layers of lead and proportional tubes. This size tower is somewhat larger than the transverse dimensions of an electromagnetic shower and contains 96% of the longitudinal energy at 20 GeV. Each layer consists of a row of fourteen proportional tubes with a 1 cm by 1 cm cross section. The tubes are formed from an aluminum extrusion with the cells open on one side. The other wall is a 3/16" thick (0.8 r.l.) piece of lead, which is specially grooved to fit over the extrusion. Before the lead is pressed on the extrusion, tungsten wires (2 mil.) are strung in each of the tubes and soldered to molded electrode strips at the ends. The resulting 5½" by 5½" proportional tube planes can be individually checked out before they are assembled into a tower. When the planes are stacked together, the tube directions are alternated to provide position information in both transverse projections.

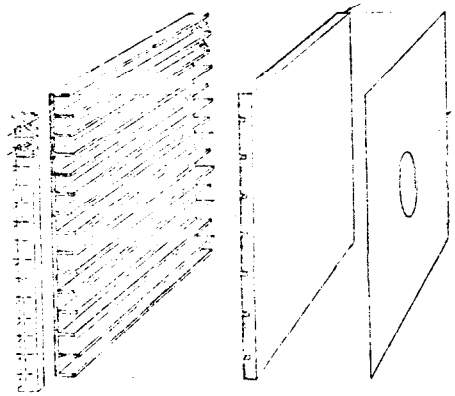

Fig. 1. Single proportional tube plane with Pb radiator for one wall.

*Work supported by US Department of Energy under Contract #DE-AC02-76ER03064.

The signals from the 280 tubes are brought to the top of the tower using G10 circuit boards in a manner similar to the use of BBQ sheets on the sides of Pb-scintillator towers. Strips on the circuit boards gang the tubes together longitudinally (along the shower direction). The longitudinal ganging is done for three separate regions in both transverse projections to improve the discrimination against charged hadrons. These regions are 6 layers, 6 layers, and 8 layers deep, starting from the upstream end of the tower. For each of these regions there are fourteen signals available corresponding to the fourteen transverse tube positions. The resulting 6 x 14 = 84 signals are further reduced to 18 or fewer per block by a resistive weighting technique described below. The tower body is run at negative high voltage so that the wires and the exposed strips will be at ground potential

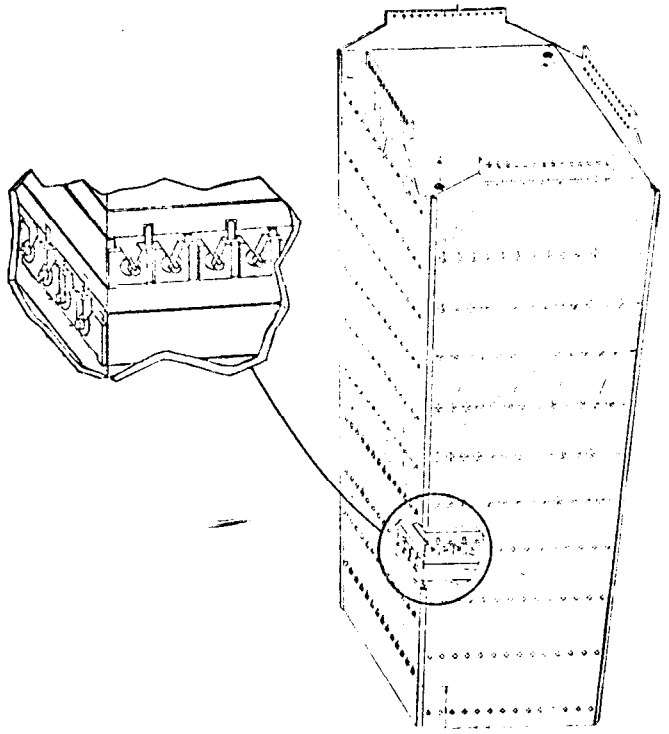

Fig. 2. Assembled shower tower. Electronics are attached on the top.

The electronics for readout and digitization of the signals are attached to the front (upstream) end of each tower. This was done so that the blocks could be cantilevered from a thick steel mounting plate, possibly the front layer of a hadron calorimeter. In addition to the preamplifier, sample and hold, and multiplexed ADC circuitry, each block has resistive weighting networks for each of the six regions. Here each of the fourteen signals is split by three parallel resistors R_A, R_B, and R_C. All fourteen R_A signals are bussed together into a preamp as are the R_B and R_C signals. The result is that three signals, S_A, S_B and S_C, instead of 14 are sampled for each region.

Transverse Resistive Weighting

N tubes → 3 signals : $\bar{x}, \bar{x}, \sigma_x$

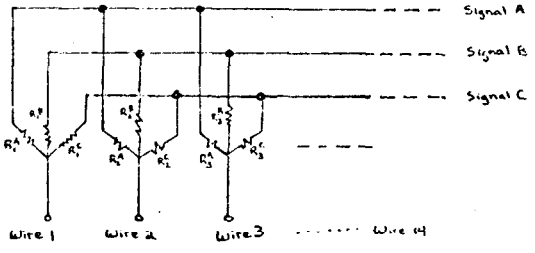

Fig. 3. Resistive weighting schematic. This is repeated for each of the six tower regions.

An "intelligent" choice of the 14 x 3 resistors R_A, R_B, R_C must be made so that the three remaining signals contain a maximum amount of information about the transverse shower distribution. An important constraint is that $1/R_A + 1/R_B + 1/R_C = 1/R_0 =$ Constant so that each tube sees the same input impedance. The resistive weighting function $f_i = R_0/R_i$ gives the fraction of the total charge in the ith preamp channel. We have chosen the following quadratic resistive weighting functions:

$$f_A = \frac{R_0}{R_A} = a(x-c)^2 + b$$

$$f_B = \frac{R_0}{R_B} = a(x+c)^2 + b \qquad (1)$$

$$f_C = \frac{R_0}{R_C} = 1 - f_A - f_B$$

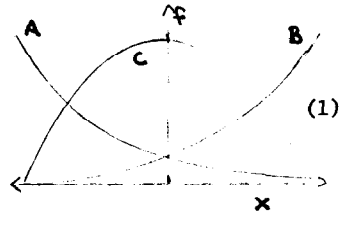

where $-7 < x < 7$ is the transverse coordinate in tubes and $a \simeq .008$, $b \simeq 0$, $c \simeq 4.5$. The effective input impedance, R_0, was 500 Ω. The choice of quadratic functions allows one to extract the zeroth, first, and second moments of the transverse energy distribution in each region; the particular choice of constants optimizes the resolution of these moments. The moments are given by

$$E = S_A + S_B + S_C$$

$$\bar{x} = \frac{S_B - S_A}{4acE}$$

$$\overline{x^2} = \frac{S_B + S_A}{2aE} - c^2 - b/a \qquad (2)$$

$$\sigma_x^2 = \overline{x^2} - \bar{x}^2$$

where E is the total energy deposited in a region, $\bar{x}$ is the centroid of the energy distribution, and σ_x is the half width of the distribution.

The latter quantity is particularly useful for distinguishing single gammas from π^0's. If E_T is the total energy deposited in a tower, then for two gamma cases:

$$m_{\gamma\gamma}^2 = E_T^2 \frac{\sigma_x^2 + \sigma_y^2}{L^2} = E_1 E_2 \theta_{12}^2 \qquad (3)$$

where L is the distance to the interaction point. However, this relationship is complicated by the intrinsic width of a single gamma. In the middle region of this detector $\sigma_x^2 + \sigma_y^2 \sim 4$ cm^2 for a single photon. This implies that π^0/γ separation is possible for $E_T/L \gtrsim 3$ GeV/m. It should be noted that the moments can be continued across tower boundaries for showers or pairs of showers which are not contained in a single tower.

We have constructed an array of four such shower towers and have tested them in the SLAC e^+ test beam. Our primary objectives were to test the resistive weighting readout scheme and to investigate the effects of the tower boundaries on the calorimeter response. We also checked the linearity of the energy response and the energy resolution of the device, but did not attempt to optimize these. The detector was run in the proportional mode at 1600 volts with a 93-7 Ar-CO_2 gas mixture. Beams of 2, 4, 10 and 16 GeV e^+ were used, and the beam spot size was less than 2mm x 2mm. By running the beam at >1 particle per pulse we were also able to simulate higher energies by observing the multiparticle peaks. This was possible because of the narrow time structure and spatial width of the beam.

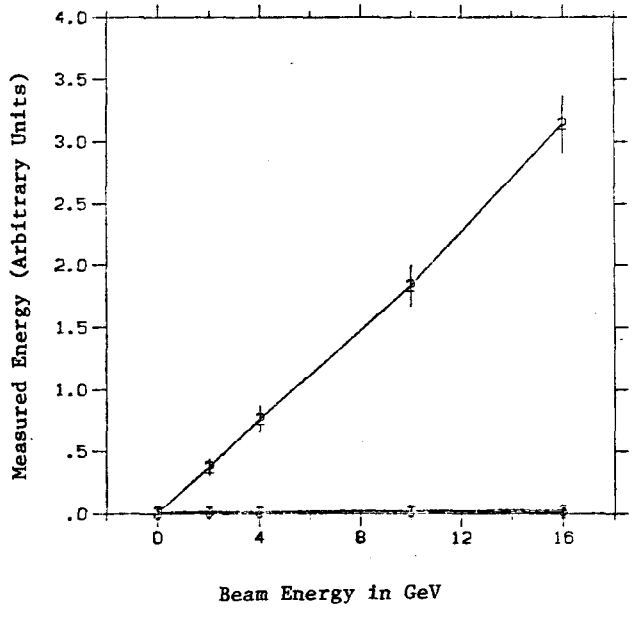

Fig. 4. Energy sweep with beam centered in block #2.

Figure 4 shows the total energy response of one tower (#2) where beams of 2, 4, 10 and 16 GeV were incident at 0° directly on the center of the tower. The absence of transverse leakage can be seen from Figure 4, where the energy deposited in the remaining three towers appears as a heavy line just above the X axis.

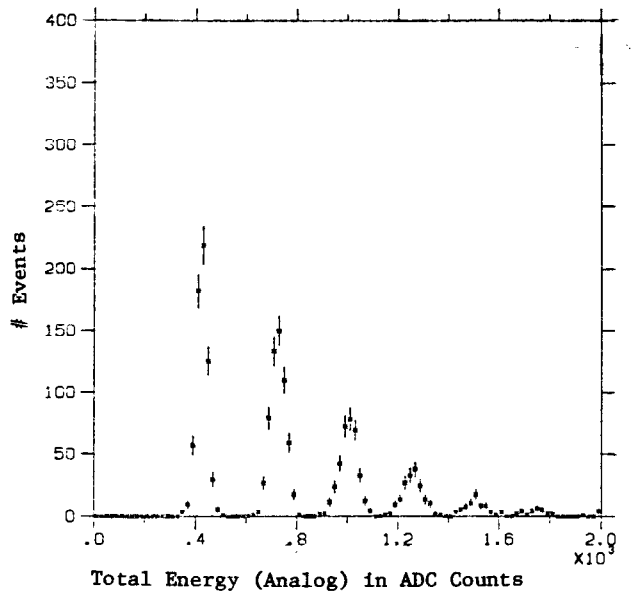

Fig. 5. Total block #2 pulse height spectrum with high intensity 16 GeV run.

The total energy spectrum from a single high intensity run at 16 GeV is shown in Figure 5. The peak positions from this run are plotted in Figure 6. The calorimeter begins to show saturation around an equivalent energy of 50 GeV.

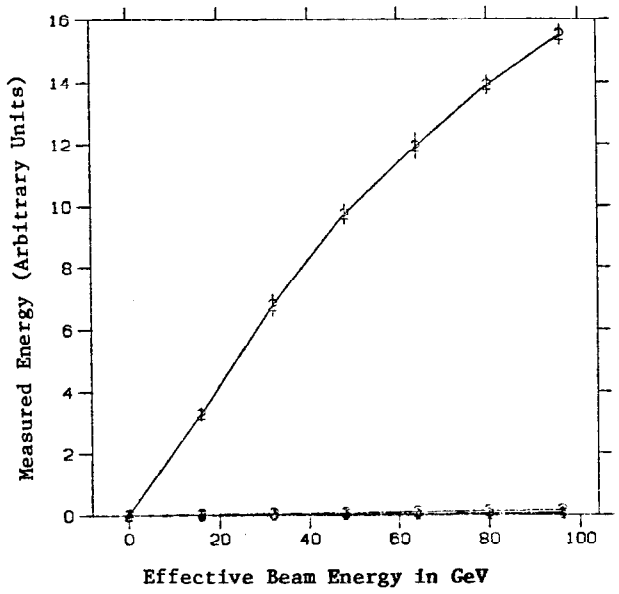

Fig. 6. Peak positions and widths from Figure 5.

The energy resolution, $\Delta E/E$, of the calorimeter is plotted against $1/\sqrt{E}$ in Figure 7 for both the energy sweep data of Figure 4 and the multiparticle peak data of Figure 5. Both data sets are reasonably well described by the relationship $\Delta E/E \simeq \frac{20\%}{\sqrt{E}} + 1\%$. The total energy signal for each tower was an analog sum of the 18 resistively weighted signals.

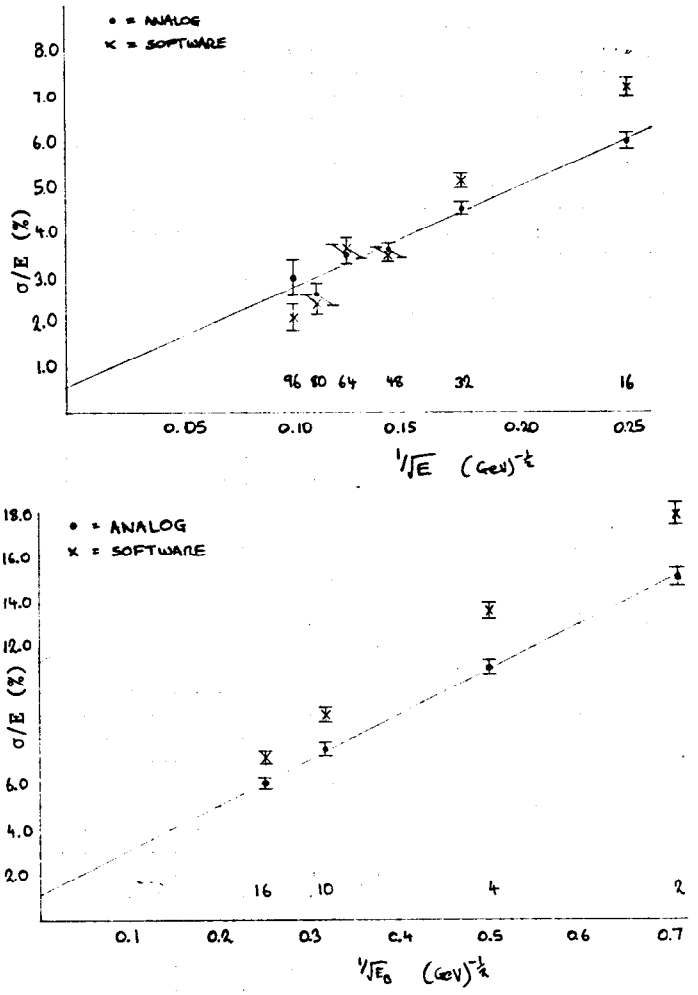

Fig. 7. Energy resolution from Figures 4 and 6 plotted vs. $1/\sqrt{E}$. Circles (crosses) are from analog (software) sum of all 18 tower signals.

We next present the data from two position sweeps made with a 10 GeV beam. In both cases the beam was swept in half inch or smaller steps in the y direction from the center of block #2 to the center of block #3. In one case the beam was at 0^{o} with respect to the tower axis, and at 20^{o} in the other. These two angles span the expected range for the applications being considered.

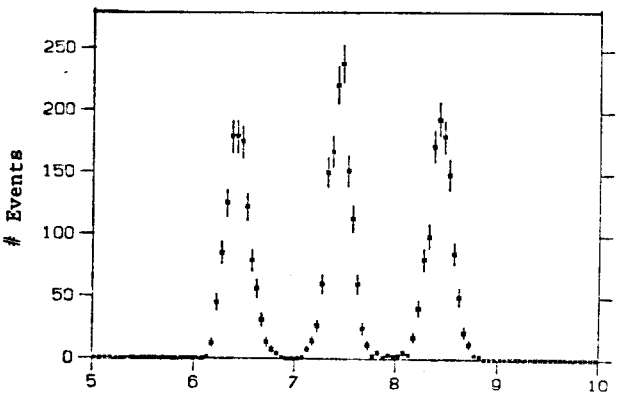

Fig. 8. Position (first moment) measurement distribution for three runs with beam position increment 1 inch.

The beam position distributions are shown in Figure 8 for three 0^o data points which were separated from each other in block 3 by 1 inch. The histogrammed quantity is the first moment, $\bar{y}$, obtained in the second longitudinal region, which includes shower maximum. The standard deviation of the peaks is 0.1 inch, which is slightly larger than the expected beam width. Because we did not have an independent beam monitor we cannot unfold our position resolution. The position resolution in the front region of the tower is about the same as the middle, while it is about twice as bad in the third region at the tail of the shower.

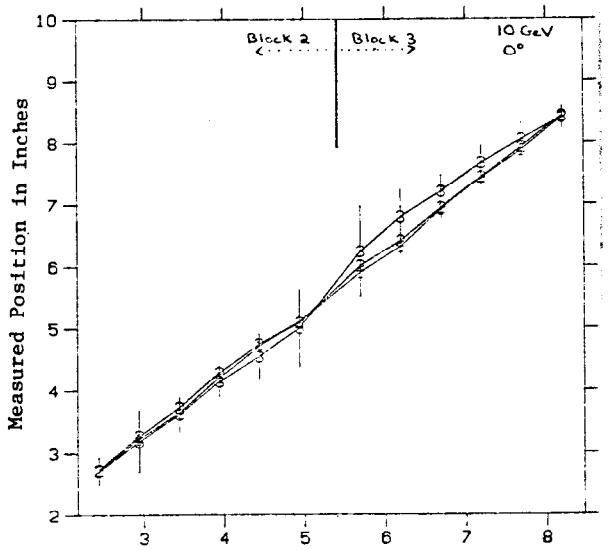

Fig. 9. First moment vs. beam position for all three tower regions with 10 GeV beam incident at 0^o.

The averages of the first moments are plotted in Figure 9 versus the beam position in y. The moments from all three longitudinal regions are superposed in the figure. Near the boundary of blocks 2 and 3 at y = 5.75" the moments are averages of the signals from both blocks. An excellent shower position measurement is obtained in all three depth regions at all positions. The data for $\bar{y}$ in the second region is plotted by itself in Figure 10. The points are seen to be in excellent agreement with the 45^o line.

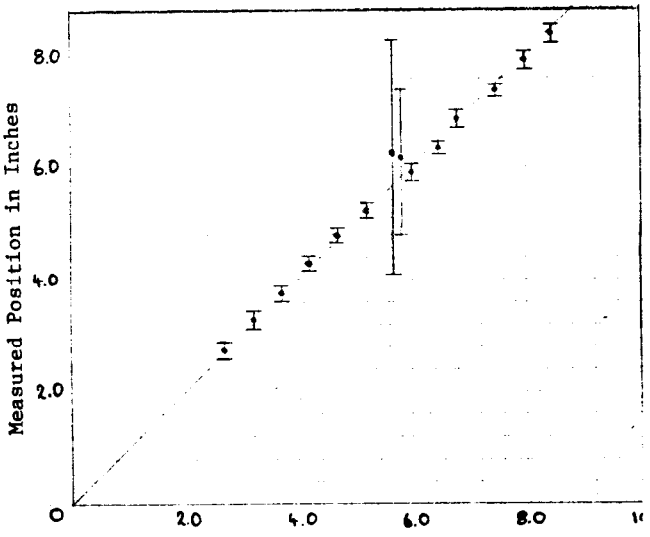

Fig. 10. First moment vs. position for region 2Y alone with 45^o line superposed.

The position measurements from the 20^o sweep are shown in Figure 11. Here the $\bar{y}$ data is especially impressive, where the points from the three regions form offset parallel lines. The offsets are consistent with tangent 20^o times the longitudinal separation of the regions. To calculate the offsets exactly it would be necessary to know the longitudinal centroid of the energy distribution for each region. The points for region 3y fall off at one end because the angled beam was no longer striking region 3.

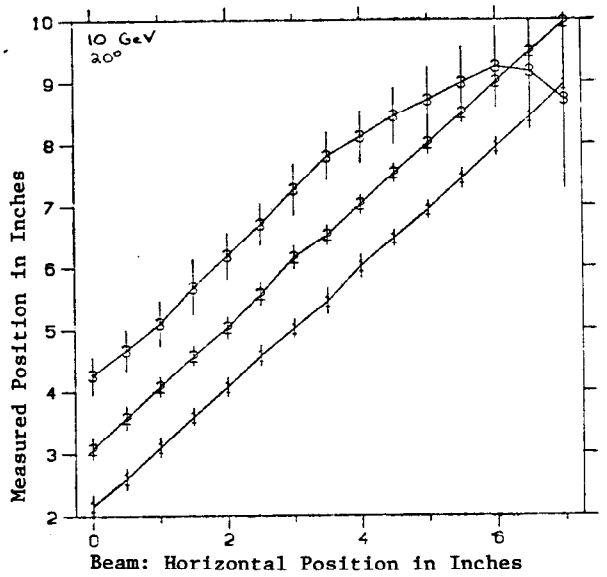

Fig. 11. Same as Fig. 9 with beam incident at 20^o.

We now turn to the results on the second moments or transverse positional variances. Figure 12 is a histogram of σ_y^2 in the second longitudinal region with the beam centered in block #3 at 0^o incident angle. The distribution of σ_y^2 in region 1 is very similar, while in region 3 it is much broader and is centered above zero. From previous shower data we would expect the shower to have $\sigma_y^2 \simeq .4$ inches square for the central region of the tower, whereas in Figure 14 our result is slightly below zero. However, if the constant b in the resistive weighting functions of Equation (1) is slightly adjusted, the scale of σ^2 will be shifted by a constant. We have already adjusted the resistive weighting constants a and c to ensure linearity of the first moments and variances with position; we did not choose to adjust b because we have no independent measurement of the shower widths in our test data. In general the resistive weighting constants needed to decode the signals differ from the "ideal" ones given by the resistor values, but seem to be consistent from region to region and block to block. Hence they only need to be calibrated once using a single tower.

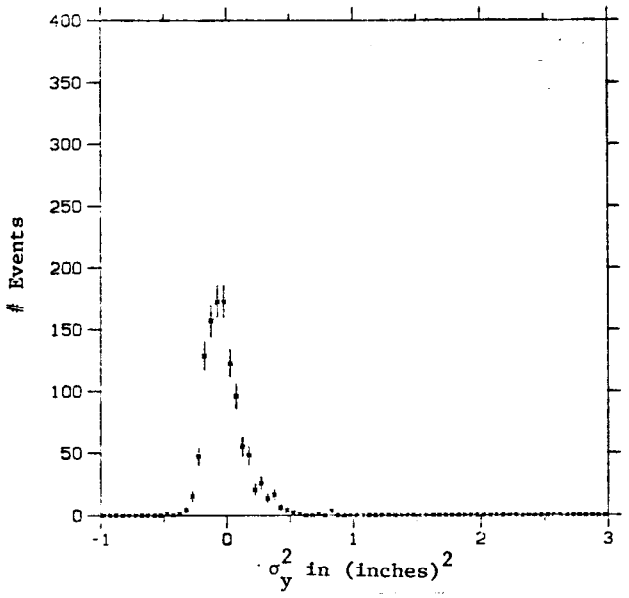

Fig. 12. Position variance distribution in region 2Y with 10 GeV, 0° beam in center of tower.

The positional dependence of the variances from all regions with the beam at normal incidence is shown in Figure 13. The values of σ^2 for longitudinal regions 1 and 2 are constant within errors, while region 3 of block #3 has a larger value of σ^2 than block #2. The jump in the value of σ^2 for region 3 is probably the result of poorer gas gain in block #3. In general one would only make use of the variance measurements in the front two regions where the shower has a dependable profile. In these regions the uncertainty is typically ±0.2 sq. in.

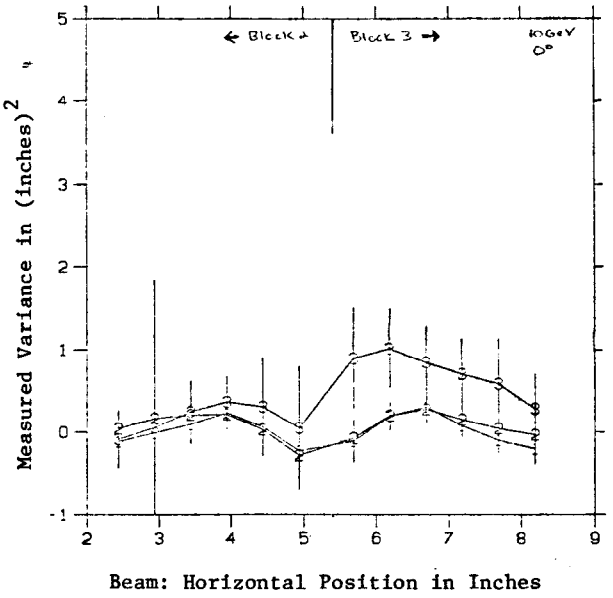

Fig. 13. Position variance (second moment) vs. position with 10 GeV beam at 0°.

As seen in Equation (3), the invariant mass for two incident gammas is dependent on $\sigma_x^2 + \sigma_y^2$. A histogram of $\sigma_x^2 + \sigma_y^2$ in region 2 of block 3 is shown in Figure 14 for the beam incident at 0°. Assuming the same resolution for a π^o and a distance L to the interaction point of 10 meters, we have sketched the expected peak for a 30 GeV π^o in the same figure. For energies below 30 GeV where the π^o peak moves to higher values of $\sigma_x^2 + \sigma_y^2$, there should be no problem separating single gammas and π^o's.

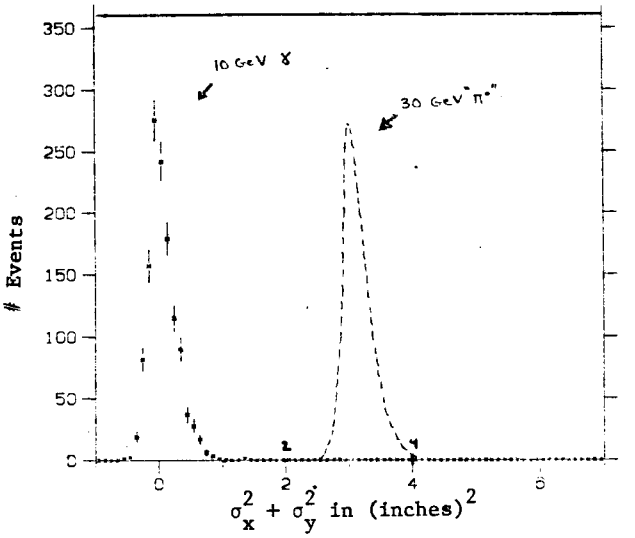

Fig. 14. Sum of sum of X and Y position variances in region 2 with 10 GeV, 0° beam. Darkened line shows expected signal for 30 GeV π^o decaying to two gammas (assuming single gamma resolution).

Finally we present the energy response of our detector as a function of position. For the 0° data, the total energy broken down by individual blocks is shown in Figure 15. The energy in block #3 was renormalized by a factor of 1.16 to balance its gain with that of block #2. There is a large dip in the response of the calorimeter at the boundary between two blocks. In fact at an angle of 0° it is possible to pass the narrow beam directly down the gap. The energy response drops practically to zero at the gap, but there is backsplash as the beam moves into the neighboring block.

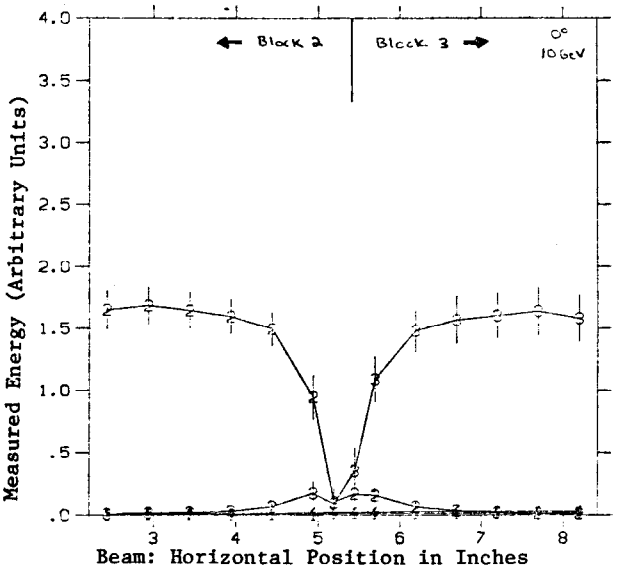

Fig. 15. Total energy response of each tower vs. position as 10 GeV, 0° beam is swept from block #2 to #3.

In Figure 16 the total energies of the x direction and y direction tubes are plotted separately. The dip at the boundary is much narrower in the case where the tubes are parallel to the boundary, namely the y-direction. Inefficiency due to field inhomogeneities at the wire ends cause this. For uniform illumination of the calorimeter at normal incidence the tubes perpendicular to boundaries have an uncorrected 20% inefficiency, while the parallel tubes are 11% inefficient. However, using the accurate position information from the resistive weighting we can correct the energy response near the boundaries so that the losses are at most a few percent. The losses are considerably smaller when the angle of incidence is finite.

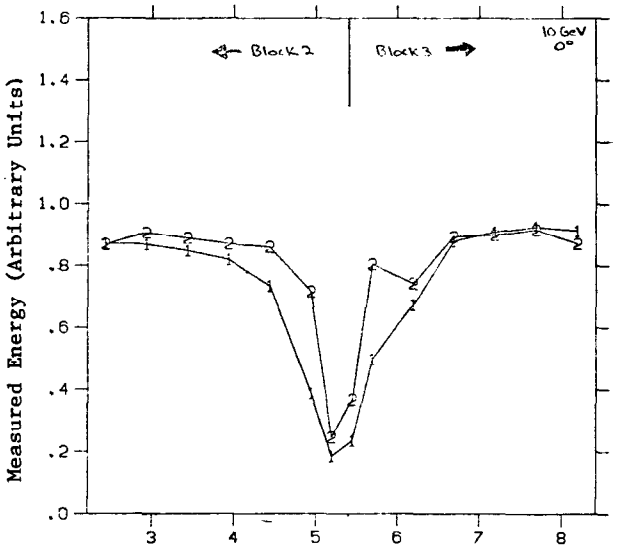

Fig. 16. Total energy response vs. position for tube perpendicular (1) and parallel (2) to the boundary with 10 GeV, 0^{o} beam.

Figure 17 shows the same quantities as Figure 16 but for the 20^{o} incident angle sweep. For this case the effect at the boundary is much smaller. In Figure 17, the raw inefficiencies for uniform illumination are now 14% for the boundary perpendicular tubes and 7% for the parallel ones. Here using the accurate position and angle information it is possible to completely correct for the boundary losses.

In conclusion the shower towers with resistive weighting provide excellent position angle information on electromagnetic showers coupled with a width measurement which allows one to discriminate between π^{o}'s and gammas. The energy response is uniform except at the tower boundaries, but here it can be corrected using the position information. Finally because of their modularity they can be used in many possible configurations.

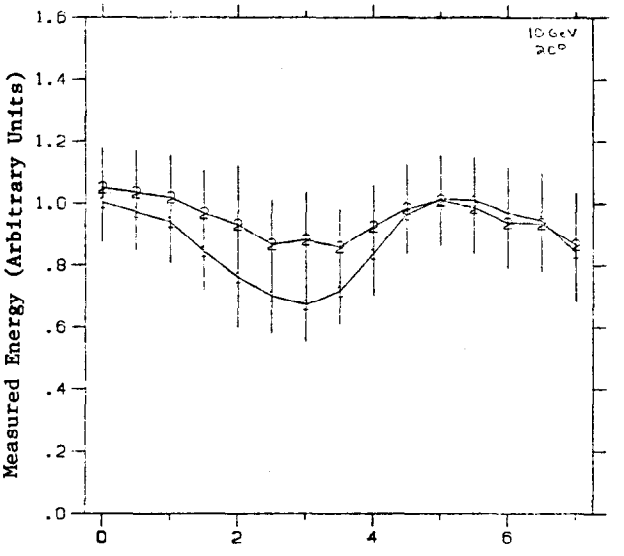

Fig. 17. Same as 16 for 20^{o} beam.